JOURNAL OF GEOPHYSICAL RESEARCH, VOL. 108, NO. A1, 1047, doi:10.1029/2002JA009487, 2003

A kinetic exospheric model of the solar wind with a nonmonotonic potential energy for the protons

H. Lamy and V. Pierrard
Institut d'Aéronomie Spatiale de Belgique, Brussels, Belgium

M. Maksimovic
LESIA, Observatoire de Paris-Meudon, France

J. F. Lemaire
Institut d'Aéronomie Spatiale de Belgique, Brussels, Belgium

Received 15 May 2002; revised 2 October 2002; accepted 25 October 2002; published 30 January 2003.

[1] In solar wind kinetic exospheric models the exobase level is defined as the altitude where the mean free paths of the coronal protons and electrons become larger than the density scale height. For the region above this exobase, kinetic exospheric models have been developed assuming that the charged particles of the solar wind move collisionless in the gravitational, electric, and interplanetary magnetic fields, along trajectories determined by their energy and pitch angle. In these models the exobase was usually chosen at a radial distance of $\sim$5–10 R_s, above which the total potential energy of the protons is a monotonic decreasing function of the radial distance. Although these models were able to explain many characteristics of the solar wind, they failed to reproduce the bulk velocities observed in the fast solar wind, originating from the coronal holes, without postulating proton and electron temperatures at the exobase in clear disagreement with recent measurements obtained with the SOHO satellite. Moreover, since the number density is lower in the coronal holes than in the other regions of the solar atmosphere, the altitude of the exobase is located deeper in the corona at a radial distance $\sim$1.1–5 R_s. At these smaller radial distances, the gravitational force is larger than the electric force acting on the protons up to a radial distance r_m. Therefore the total potential energy of the protons is first attractive (increasing with altitude) and then repulsive (decreasing with altitude). We describe a new exospheric model with a nonmonotonic total potential energy for the protons and show that lowering the altitude of the exobase below the maximum of the potential energy accelerates the solar wind protons to large velocities. Since the density is lower in coronal holes and the exobase is at lower altitude, the solar wind bulk velocities predicted by our new exospheric model are enhanced to values comparable to those observed in the fast solar wind. *INDEX TERMS:* 2164 Interplanetary Physics: Solar wind plasma; 2169 Interplanetary Physics: Sources of the solar wind; 7827 Space Plasma Physics: Kinetic and MHD theory; 7511 Solar Physics, Astrophysics, and Astronomy: Coronal holes; *KEYWORDS:* solar wind, coronal holes, kinetic models, nonmonotonic potential, kappa distributions

Citation: Lamy, H., V. Pierrard, M. Maksimovic, and J. F. Lemaire, A kinetic exospheric model of the solar wind with a nonmonotonic potential energy for the protons, *J. Geophys. Res.*, *108*(A1), 1047, doi:10.1029/2002JA009487, 2003.

1. Introduction

[2] In solar wind kinetic exospheric models the exobase is the altitude which separates a collision dominated region where a fluid approximation is valid and the exosphere where the plasma is assumed to be fully collisionless. In the exosphere the trajectory of a charged particle is therefore only determined by the conservation of the total energy

$$E = \frac{mv^2}{2} + m\phi_g + ZeV(r) = \mathrm{cst} \tag{1}$$

and of the first adiabatic invariant

$$\mathcal{M} = \frac{mv^2 \sin^2\theta}{2B} = \mathrm{cst}, \tag{2}$$

0148-0227/03/2002JA009487$09.00

provided that the guiding center approximation is valid. In these equations, v is the velocity of the particle, m is its mass, and Ze is its charge. $\phi_g = -MG/r$ is the gravitational potential (M denotes the mass of the Sun, G denotes the gravitational constant, and r is the radial distance) and $V(r)$ is the interplanetary electrostatic potential. θ is the pitch angle of the particle, i.e., the angle between the magnetic field $\mathbf{B}(\mathbf{r})$ and the velocity vector $\mathbf{v}$ of the particle. For simplicity and without loss of generality we assume that the magnetic field lines are radial, i.e., that the angular velocity of the Sun is zero. It has been shown by *Pierrard et al.* [2001] that this simplification does not affect significantly the distributions of densities and bulk speeds in the present type of modelization.

[3] The correct determination of the radial profile of the interplanetary electrostatic potential, $V(r)$, is the key point in all the solar wind kinetic/exospheric models. Because of their mass, the electron tends to escape more easily from the Sun's gravitational field than the ions. To avoid charge separation and currents on large scales in the exosphere, the electrostatic potential gives therefore rise to a force which attracts the electrons towards the Sun and repels the protons. Actually, at the scale of the plasma Debye length, $V(r)$ is induced by a slight charge separation between electrons and ions, which, apart the gravitational effect mentioned above, is also due to magnetic forces and thermoelectric effects.

[4] For the solar wind electrons the gravitational potential is negligible at all the radial distances in the exosphere. The total potential energy of an electron $m_e\phi_g(r) - eV(r) \approx - eV(r)$ is therefore an increasing function of the radial distance r. For the protons, however, it is much more complicated since the gravity cannot be neglected for those particles. In earlier exospheric models of the solar wind [*Lemaire and Scherer*, 1971a, 1973; *Pierrard and Lemaire*, 1996; *Maksimovic et al.*, 1997b, 2001], the exobase level r_0 was taken at such radial distance (between 5 and 10 solar radii R_s) that the total potential energy of a proton $m_p\phi_g(r) + eV(r)$ is a monotonically decreasing function of r. All the protons are submitted to a repulsive total force and are on escaping trajectories.

[5] This latter condition is no more valid when the exobase location is closer to the surface of the Sun, which actually happens in the coronal holes. In that case there appear ballistic protons, for which the total potential energy is attractive. With such conditions, a maximum for the proton total potential energy appears at a radial distance r_m located close to the Sun (between 1.1 and 7 R_s). Above r_m the electrostatic (repulsive) force acting on a proton becomes larger than the gravitational (attractive) force. Indeed the gravitational force decreases as r^{-2} while the outward electric field decreases more slowly with r.

[6] As we mentioned previously, the earlier exospheric solar wind models were developed with an exobase level taken above r_m, so that the total potential energy was always a monotonic decreasing function of the radial distance for the protons and a monotonic increasing function for the electrons. Exospheric models of the solar and polar wind have been reviewed by *Lemaire and Scherer* [1973], *Fahr and Shizgal* [1983], and *Lemaire and Pierrard* [2001]. Here we extend these exospheric models to the case where the exobase r_0 is lower than r_m so that the total potential energy of the protons is attractive below r_m and repulsive above r_m.

[7] The aim of this study is to show that extended exospheric models can reproduce the main characteristics of the fast solar wind originating in coronal holes. In the next section we present the details of this new kinetic exospheric model of the solar wind. The methods used to determine the parameters of the model and to calculate the self-consistent electrostatic potential distribution are discussed in section 3. In section 4 we present some applications showing how the solar wind can be accelerated to higher bulk velocities when the exobase level is located below r_m. It is shown that this model explains the acceleration of the fast solar wind, without the need of additional energy and momentum deposition in the corona.

2. Generalization of the Kinetic Exospheric Models

[8] In this section we describe how to calculate the main macroscopic quantities (density, field-aligned flux, parallel and perpendicular pressures, and energy flux) of the protons and electrons in the solar wind by integrating their velocity distribution functions (VDF) for the case of a global potential energy of the protons with a maximum at a distance r_m and an exobase level r_0 located below r_m. These integrations can equivalently be performed in the velocity space [*Lemaire et Scherer*, 1971b, hereafter LS71] or in the [E, $\mathcal{M}$] space [*Khazanov et al.*, 1998]. The dimensionless total potential energy of a particle is defined by $\psi(r) = \frac{m\phi_g+ZeV(r)}{kT_0}$, where T_0 is the plasma temperature at r_0, assumed to be identical for protons and electrons.

2.1. Exobase Level for Coronal Holes

[9] The exobase altitude r_0 is usually defined as the distance from the Sun where the Coulomb mean free path λ becomes equal to the local density scale height H:

$$H = \left(-\frac{d\ln n_e}{dr}\right)^{-1}, \tag{3}$$

where n_e is the electron density determined from eclipse observations as was done in the work of *Lemaire and Scherer* [1971a]. For the coronal temperatures and densities considered in this paper, the classical *Spitzer*'s [1962] proton deflection mean free path is

$$\lambda_p \sim 7.2 \times 10^7 \frac{T_p^2}{n_e}, \tag{4}$$

where T_p is the proton temperature (MKSA units). In the equatorial streamers, the density is large so that r_0 is generally located between 5 and 10 solar radii and therefore generally above r_m. However, in the coronal holes the density is lower than in the other regions of the solar corona and the exobase is therefore located deeper into the solar corona.

2.2. Electrons

[10] For the electrons, $\psi(r)$ is always monotonically increasing with radial distance. The Lorentzian exospheric model [*Pierrard and Lemaire*, 1996] has been used to take into account the effects of the suprathermal tails observed at large distance in the electrons VDF of the high-speed solar

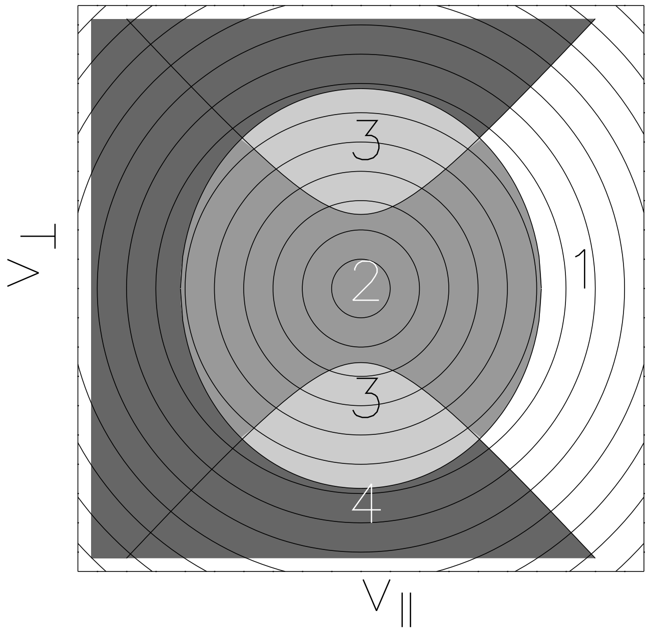

Figure 1a. Schematics of the regions in [$v_{\|}$, $v_{\perp}$] space for the case of an attractive total potential. The different classes of particules are (1) escaping particles, (2) ballistic particles, (3) trapped particles, and (4) incoming particles. This situation arises for the electrons from the exobase level r_0 to ∞ and for the protons from r_0 to r_m, the radial distance where the total potential energy of the protons has a maximum.

wind [*Maksimovic et al.*, 1997b]. The electrons moving along a magnetic field line may belong to different classes of orbits: the escaping electrons (which have a kinetic energy larger than the escape energy), the ballistic electrons (which have not enough kinetic energy to escape and have a turning point in the exobase; they fall back into the corona), the trapped electrons (which have one magnetic mirror point and one turning point in the exosphere; they bounce continuously up and down along a magnetic field line), and the incoming electrons (whose VDF is assumed to be empty, since no particles are assumed to return from the interplanetary space to the Sun). In Figures 1a and 1b, these four classes of orbits are illustrated in velocity space and in the [E, $\mathcal{M}$] space, respectively.

[11] In the Lorentzian model of *Pierrard and Lemaire* [1996] and *Maksimovic et al.* [1997b], the electron VDFs were assumed to possess an enhanced population of suprathermal electrons characterized by small values of the electrons kappa index, in agreement with the observations [*Maksimovic et al.*, 1997a]. In the hot equatorial regions, the electron VDFs are closer to the Maxwellian equilibrium corresponding to $\kappa_e = \infty$. This Lorentzian exospheric model rather satisfactorily accounts for the main features of the solar wind. Nevertheless, it was unable to reproduce the large speeds (~700–800 km/s) sometimes observed in the high speed solar wind without postulating unreasonably large coronal temperatures ($T_e = 2 \times 10^6$ K) in disagreement with the recent SOHO measurements ($T_e \sim 10^6$K, e.g., *David et al.* [1998]). In the present work we show how it is possible to reach such velocities by modifying both the κ_e value and the position of the exobase r_0, without the need of excessively high coronal temperatures.

2.3. Protons in [r_0, r_m]

[12] The expressions of the moments of the proton VDF have been generalized to take into account a nonmonotonic distribution of their potential energy. Such a potential energy has been treated by *Lemaire* [1976] for the case of a rotating ion-exosphere. However, the case of the solar wind is more complicated, since the radial distance r_m cannot be calculated analytically. Indeed, the Pannekoek-Rosseland potential distribution considered by *Lemaire* [1976] is not valid for open field lines when the plasma is not in hydrostatic equilibrium, and the electric field has to be calculated self-consistently by successive iterations. The mathematical method to determine the position of the maximum of the proton potential, r_m, is explained in section 3.

[13] The VDF of the protons is a truncated maxwellian, like in previous exospheric models. Indeed, *Maksimovic et al.* [1997b] assumed a Lorentzian VDF only for electrons since solar wind bulk speeds are relatively insensitive to the existence of protons suprathermal tails.

[14] From r_0 to r_m, $\psi(r)$ is monotonically increasing with radial distance, and we simply adapted the model described in *LS71* by setting the position of the maximum of ψ(r) at a finite distance, r_m, instead of at infinity. The different classes of proton orbits are illustrated in Figures 1a and 1b.

[15] The number density n, the flux of particles F, the parallel and perpendicular momentum flux $P_{\|}$ and $P_{\perp}$, respectively, and the energy flux parallel to the magnetic field ϵ, are given in Appendix A for the different classes of particles by integrating the VDF over the appropriate regions of the velocity space, as was done in LS71. Note that we have modified some mathematical forms initially introduced in this older study in order to use only the complementary error function, erfc(x), and the Dawson's integral, $\mathcal{D}(x)$, instead of their $K_m(x)$ and $W_m(x)$ functions. Indeed, asymptotic expressions for the former functions can be evaluated more precisely when their arguments are large [*Scherer*, 1972], i.e., when the altitude r is close to r_m. All these procedures were carefully cross-checked with the equivalent method developed by *Khazanov et al.* [1998] in

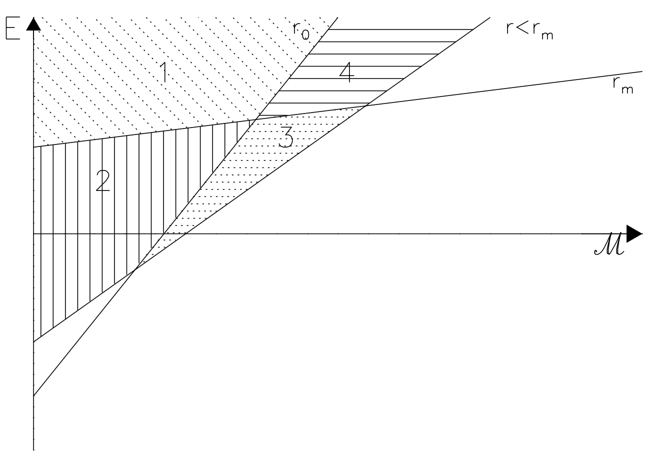

Figure 1b. Same as in Figure 1a but mapped in the [E, $\mathcal{M}$] space. The different curves in Figure 1a map into straight lines in this equivalent formulation.

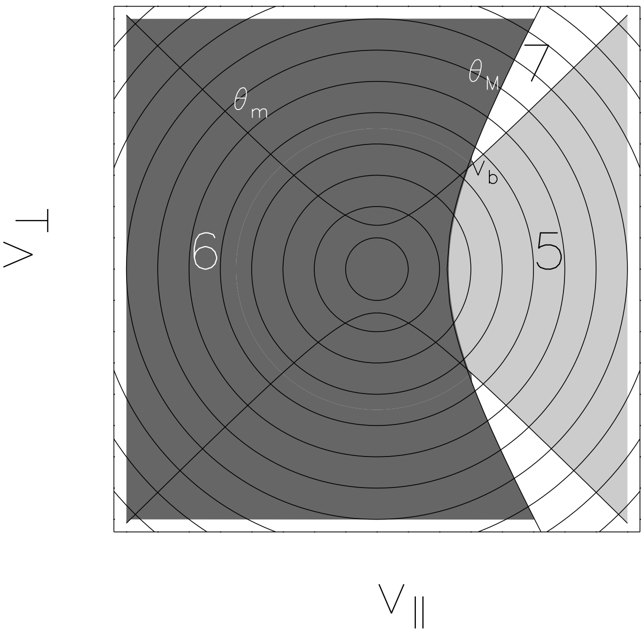

Figure 2a. Schematics of the regions in $[v_{\|}, v_{\perp}]$ space for the case of a repulsive potential beyond r_m, the radial distance of the maximum of the proton total potential energy. The escaping particles (5) are those which have enough kinetic energy to overcome the maximum of the total potential and which are not magnetically reflected. The unshaded region (7) is an empty region and results from the fact that not all the protons from the exobase are able to reach r_m. The incoming particles (6) are assumed to be missing owing to presumed absence of pitch angle scattering in the exosphere. v_b is the velocity corresponding to the intersection of the $\theta = \theta_m\ (v)$ and $\theta = \theta_M\ (v)$ curves.

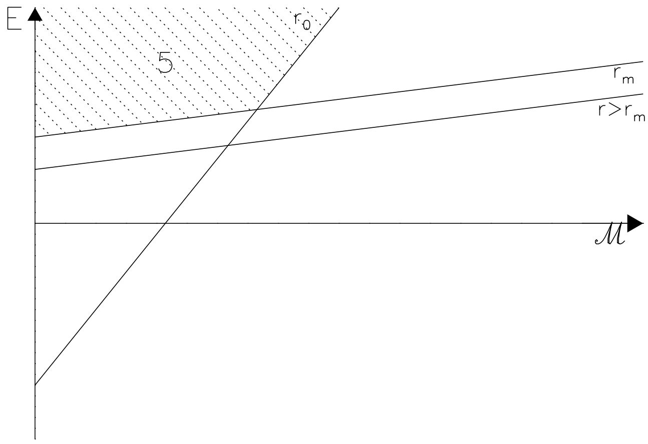

Figure 2b. Same as in Figure 2a but represented in $[E, \mathcal{M}]$ space.

the $[E\text{-}\mathcal{M}]$ paradigm, using their formulae (9) to (11) and (D2) to (D8). Note that there is a small error in their formula (D6) that can be easily found by starting with their general formula (9e).

2.4. Protons in $[r_m, \infty]$

[16] From r_m to infinity, $\psi(r)$ decreases monotonically. Since only protons with sufficiently high energy can reach r_m, the flux of escaping particles is smaller than that used in the earlier exospheric models for which the exobase was assumed to be located beyond r_m. This is illustrated in Figure 2a where the shaded area corresponds to escaping particles, accelerated upwards by the repulsive potential distribution. The unshaded area is a new empty region of velocity space while the black region corresponds to the missing incoming particles. Figure 2b illustrates the situation in the $[E, \mathcal{M}]$ space used in the study of *Khazanov et al.* [1998].

[17] The calculation of the different moments of the VDF of protons beyond r_m are given in details in Appendix B.

3. Determination of the Model Values of r_m, V_0, and V_m and of the Radial Distribution of the Electrostatic Potential

[18] The moments of the VDF in the solar wind depend on the electrostatic potential distribution $V(r)$. In earlier exospheric models the only unknown parameter was the value of the electrostatic potential at the exobase V_0 which was imposed so that the flux of escaping protons is equal to the flux of escaping electrons. Otherwise, there would be a continuous positive charge accumulation at the base of the corona and a continuous increase of negative charges at large radial distances. The equilibrium value of V_0 depends on the temperature at the exobase T_0 and on the value of the kappa index κ_e, characterizing the hardness of the spectrum of the suprathermal electrons.

[19] Now that the total potential energy of protons has a maximum, we have three unknown parameters in the model: V_0 is the value of the electric potential at the exobase, V_m is its value at r_m, and r_m is the altitude of

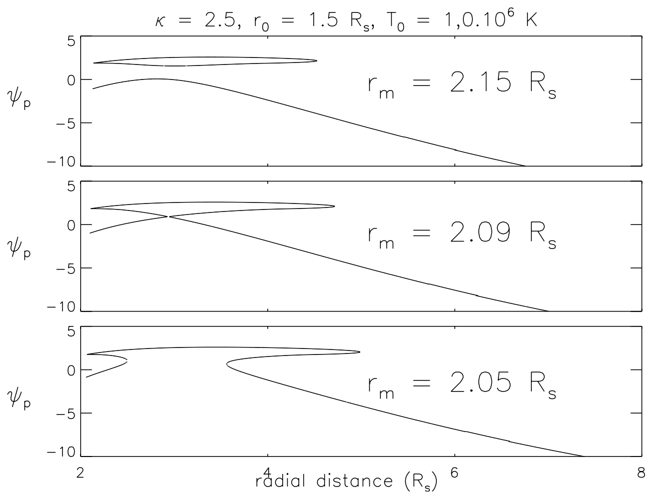

Figure 3. The search of the critical value of r_m illustrated for the case $\kappa_e = 2.5$, $r_0 = 1.5$ R$_s$ and $T_0 = 1.0 \times 10^6$ K. The three panels show, for three different values of r_m, all the possible solutions for ψ_p, the dimensionless total potential of the protons, that satisfy the quasi-neutrality equation. In the top and bottom panels, the values of r_m are respectively smaller and larger than the critical value of r_m for which the solution is continuous in the whole range of altitudes between r_0 and ∞. This solution is illustrated in the middle panel for which the value of r_m is close enough to ensure the continuity of the solution.

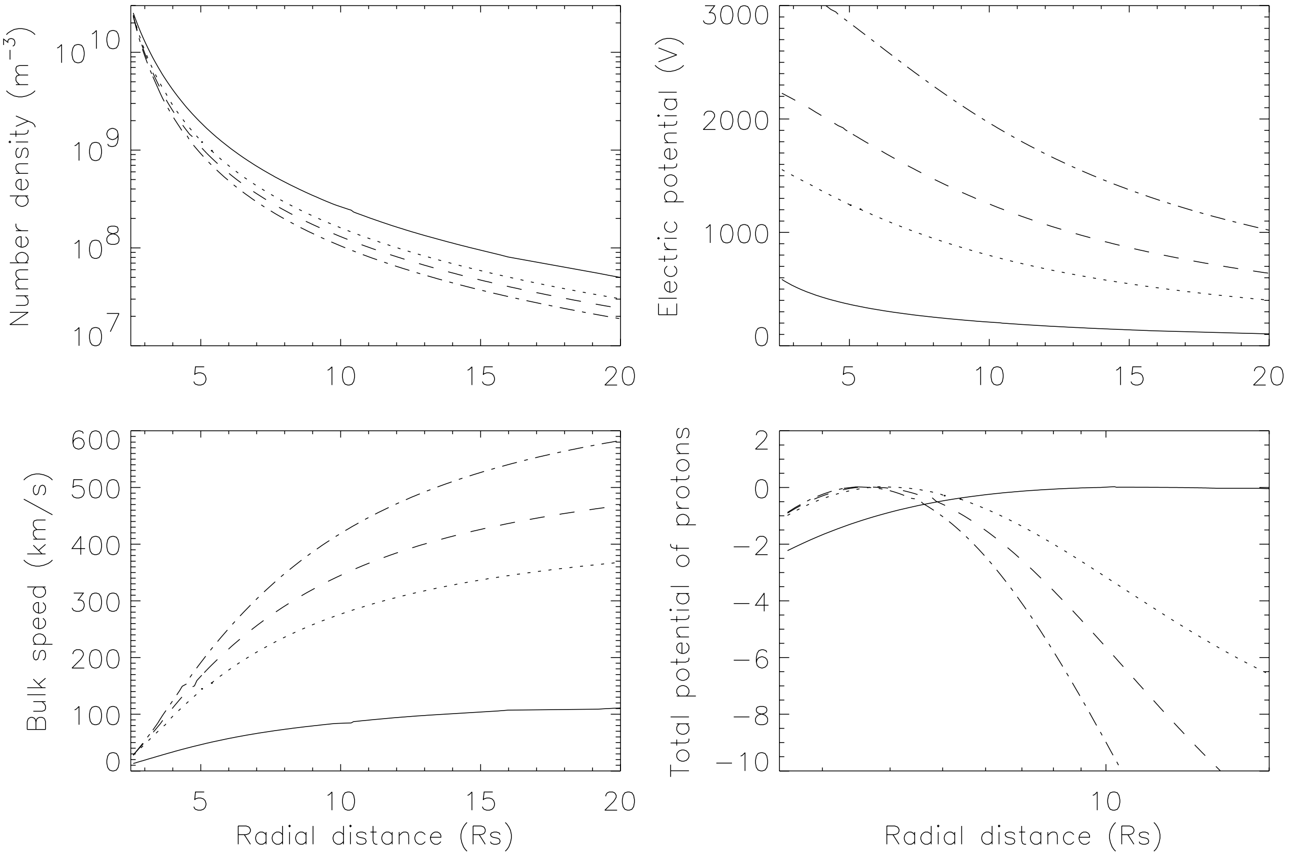

Figure 4. Influence of a change in the value of the kappa index κ_e of the electron VDF on n, the number density, V, the electrostatic potential, and u, the bulk speed of the solar wind for the case $r_0 = 2.5\ R_s$ and $T_0 = 1.0 \times 10^6$ K. The total potential of the protons is given in the lower right panel and is normalized so that it is zero at r_m. The $\kappa_e = 1000$ curve (solid line), close to the Maxwellian case, is drawn together with three other curves corresponding to electrons VDF characterized by more and more suprathermal electrons: $\kappa_e = 3$ (dotted line), $\kappa_e = 2.5$ (dashed line) and $\kappa_e = 2.2$ (dashed-dotted line).

the maximum of the proton potential. V_0 determines the potential barrier that the electrons have to overcome in order to reach infinity with a zero residual velocity. V_m corresponds to the potential barrier for the protons. To determine these three parameters simultaneously, we follow an iterative procedure originally developed by *Jockers* [1970]: fixing a value of r_m, the values of V_0 and V_m are calculated by solving the electrical quasi-neutrality equation and the zero current condition with an iterative Newton-Raphson method.

$$n_p(r = r_m, V_0, V_m, r_m) = n_e(r = r_m, V_0) \tag{5}$$

$$F_p(r = r_m, V_0, V_m, r_m) = F_e(r = r_m, V_0). \tag{6}$$

[20] In equation (5), n_e and n_p are the electron and proton densities at $r = r_m$, and in equation (6), F_e and F_p are the field-aligned fluxes for electrons and protons at $r = r_m$. This approach is a generalization of the work described in appendix 3 of *Jockers* [1970]. Indeed, *Jockers* [1970] used Maxwellian VDF for electrons and protons while we are using a Lorentzian VDF for the electrons. It has been verified that when taking $\kappa_e \sim \infty$, we recover the same results as those described in his model I.

[21] For the fixed value of r_m, once we have determined the values of V_0 and V_m, the radial distribution of $V(r)$ can be calculated by solving numerically the electrical quasi-neutrality equation at any radial distance: $n_e(r) = n_p(r)$. Note that the formulae for $n_p(r)$ are different below or above r_m. For $r > r_m$, this equation has one or three mathematical solutions depending on the values of r_m and r (see Figure 3 for an example). Obviously, the physically meaningful solution must start from $\psi_p(r_m)$ and continuously decrease to infinity. Such a solution only exists for a "critical" value of r_m. Indeed, if r_m is too small, there is a range of radial distances above r_m where no real solution exists. On the other hand, if r_m is too large, the solution is not continuous. An example of this behaviour is given in Figure 3.

4. Radial Distribution of Solar Wind Plasma

[22] In this section we present the numerical results obtained with the generalized model when the exobase r_0 is lower than r_m. We examine the effect of the model parameters that influence most significantly the value of the solar wind bulk velocity at large distance. The aim is to identify for which range of values one obtains bulk velocities observed in the high speed solar wind. These model parameters are (1) the index κ_e of the Lorentzian

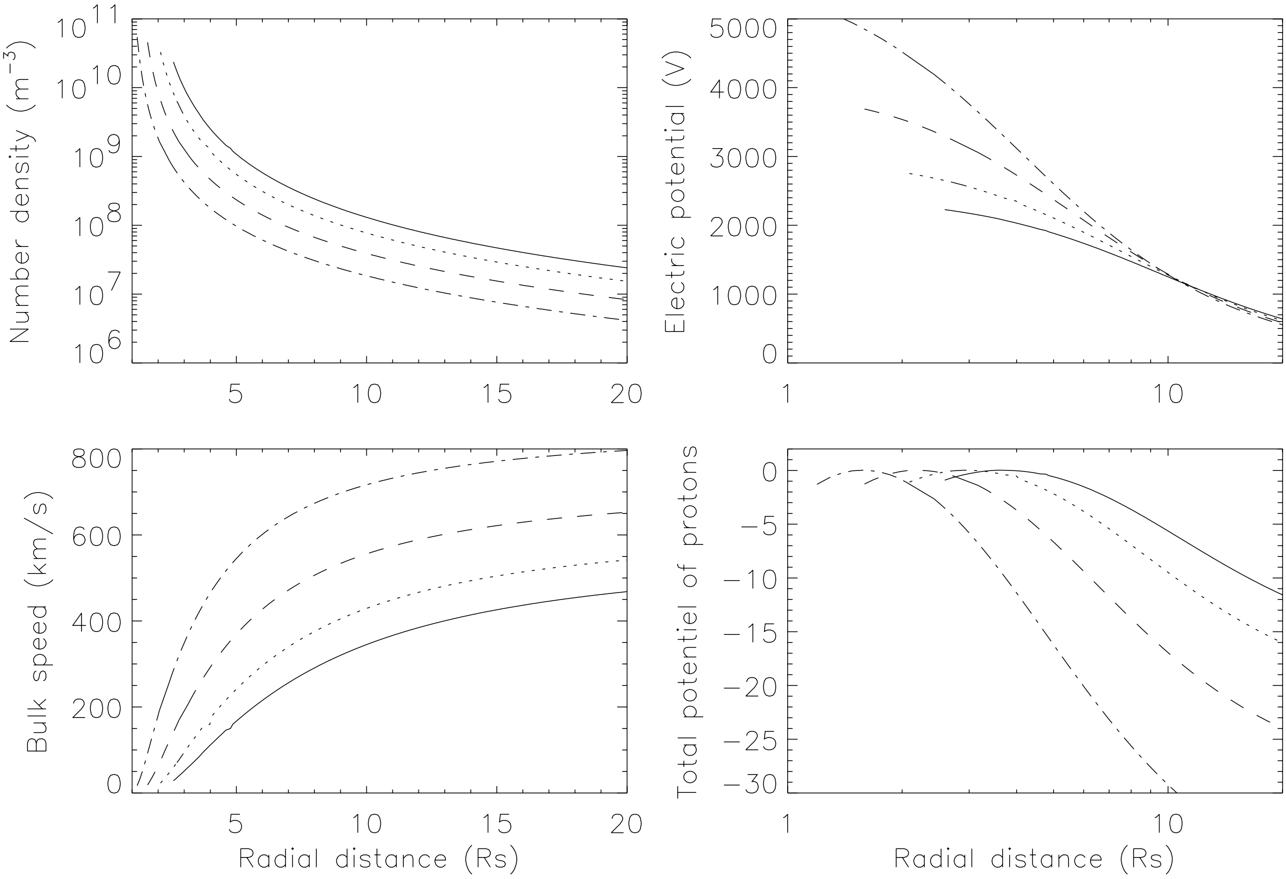

Figure 5. Influence of the exobase radial distance r_0 on the same physical variables as in Figure 4, for $\kappa_e = 2.5$ and $T_0 = 1.0 \times 10^6$ K. Four different values of r_0 are assumed: $r_0 = 2.5$ R$_s$ (solid line), $r_0 = 2.0$ R$_s$ (dotted line), $r_0 = 1.5$ R$_s$ (dashed line), and $r_0 = 1.1$ R$_s$ (dashed-dotted line). The density at the exobase, n_0, has been evaluated in order to satisfy equations (3) and (4). The solar wind is more strongly accelerated and reaches larger asymptotic values at infinity when the exobase level is located deeper in the corona.

electron VDF, (2) the level of the exobase r_0, and (3) the temperature at the exobase T_0. In Figures 4 to 6 the plasma density $n(r)$, the electrostatic potential $V(r)$, the bulk speed $u(r)$, and the total normalized potential of the protons $\psi_p(r)$ are represented versus the radial distance up to 20 R$_s$. The asymptotic bulk speed at a distance of 1 AU are reported in Tables 1 to 3 together with the fitted values of r_m, V_0, and V_m. The density at the exobase is $n_e = n_p = n_0 = 3 \times 10^{10}$ m^{-3} and was assumed identical for all models, except when we vary the radial distance of the exobase. In that case, n_0 was calculated in order to satisfy the equality of the mean free path of protons and the density scale height (equations (3) and (4)), given that T_0 was assumed constant.

4.1. Influence of Kappa Index κ_e

[23] Let us assume that the exobase is located at a fixed distance, $r_0 = 2.5$ R$_s$ and that the temperature at the exobase is $T_0 = 1.0 \times 10^6$ K. We examine how the value of κ_e influences the solar wind macroscopic quantities defined above and in particular the bulk speed $u(r)$. The values of κ_e considered in Figure 4 are listed in Table 1. They include $\kappa_e = 1000$, corresponding almost to the Maxwellian case ($\kappa_e = \infty$). The other κ_e indexes are compatible with Ulysses observations [*Maksimovic et al.*, 1997a].

[24] Figure 4 and Table 1 indicate that the lower the κ_e index, the higher the bulk speed at 1 AU. This is a direct consequence of the larger value of V_0, the exobase potential, shown in upper right panel of Figure 4. Indeed, in order to keep equal the escape flux of protons and electrons, a higher potential difference between the exobase and infinity is required. This effect has already been studied and discussed by *Maksimovic et al.* [1997b] but the asymptotic values of $u(r)$ reached here are slightly larger than in this previous study because of the fact that the proton flux is reduced at altitudes below r_m where there are ballistic protons.

4.2. Influence of the Exobase Level r_0

[25] The κ_e index of the electron VDF and T_0, the temperature at the exobase are fixed: $\kappa_e = 2.5$ and $T_0 = 1.0 \times 10^6$ K. We examine how the bulk speed $u(r)$ depends on the radial distance of the exobase r_0. The density at the exobase is modified accordingly to equations (3) and (4). The values of r_0 chosen in Figure 5 are reported in Table 2 corresponding to typical density profiles postulated in coronal holes regions [*Whitbroe*, 1988; *Maksimovic et al.*, 1997b].

[26] Figure 5 and Table 2 indicate that the electrostatic potential difference for the electrons is very sensitive to the position of the exobase and is over 5000 Volts when the

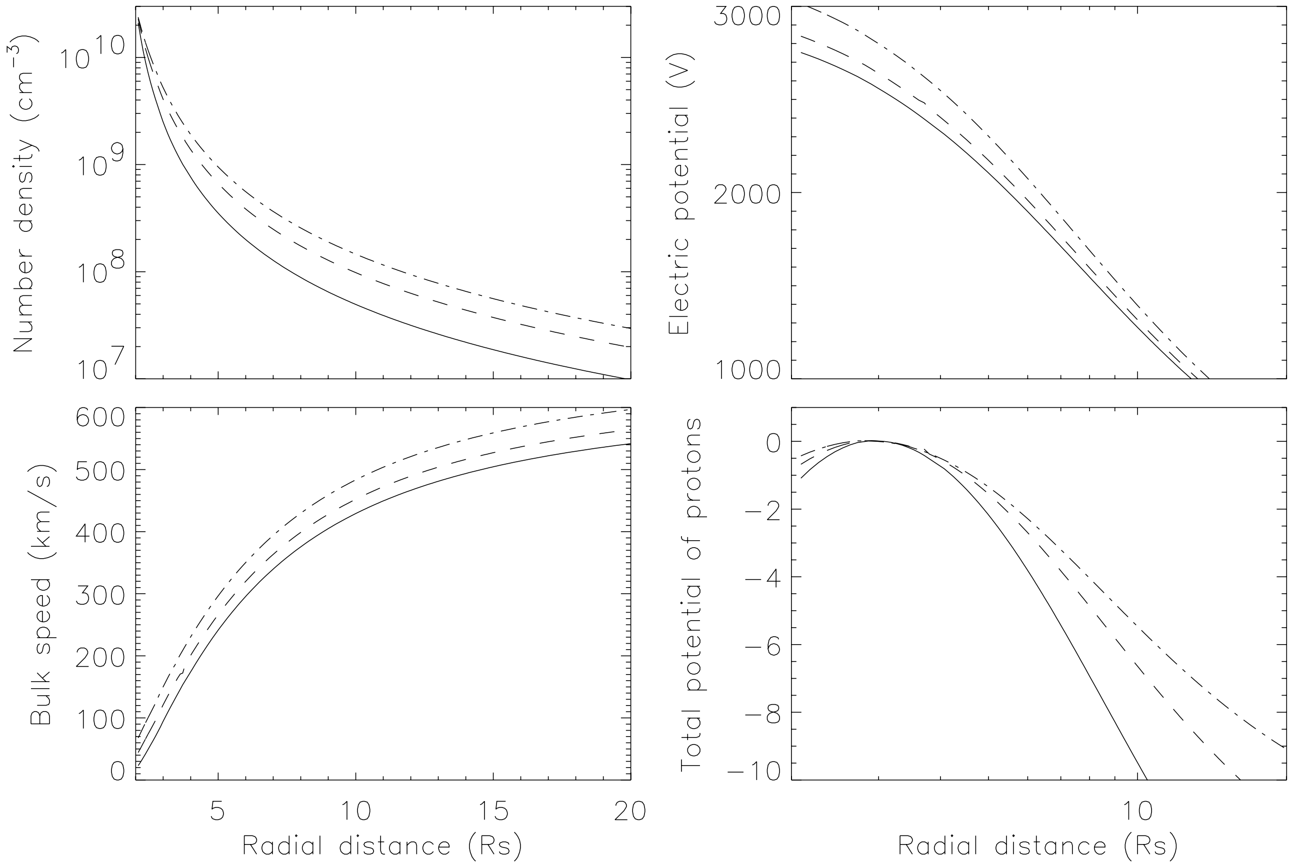

Figure 6. Influence of the exobase temperature T_0 on the same physical variables as in Figure 4 for $\kappa_e = 2.5$ and $r_0 = 2.0$ R$_s$. Three values of T_0 are assumed: $T_0 = 1.0 \times 10^6$ K (solid line), $T_0 = 1.5 \times 10^6$ K (dashed line), and $T_0 = 2.0 \times 10^6$ K (dashed-dotted line). The solar wind velocity at large distance is not as sensitive to the exobase temperature, T_0, as it is to the exobase radial distance, r_0.

exobase is located below 1.1 R$_s$. Consequently, the solar wind is more strongly accelerated when r_0 is drastically reduced. Observed high-speed solar wind bulk velocities are obtained for low enough exobase levels. Indeed, the outward proton flux is again reduced and a larger exobase potentiel difference is required to equalize the escape fluxes of electrons and ions.

4.3. Influence of the Exobase Temperature, T_0

[27] The κ_e index of the electron VDF and the altitude of the exobase are fixed: $\kappa_e = 2.5$ and $r_0 = 2.0$ R$_s$. We examine how the bulk speed $u(r)$ depends on the temperature at the exobase, T_0. The results are displayed in Figure 6 and in Table 3. It can be seen that even with an unrealistically high temperature of 2×10^6 K at the exobase, the solar wind bulk velocity at large distance never reaches values as high as in the cases when the exobase altitude and/or κ_e are lowered. This clearly shows that T_0 is not the key parameter leading to fast speed streams, a conclusion already claimed by *Lemaire and Scherer* [1971a].

5. Summary and Perspectives

[28] In the present study we describe a new exospheric model of the solar wind where a non monotonic radial distribution of the proton potential energy is taken into

Table 1. Values of r_m, the Radial Distance of the Maximum Total Potential Energy of the Protons, V_0, the Exobase Electric Potential, V_m, the Electric Potential at $r = r_m$ and u, the Solar Wind Bulk Speed at 1 AU Obtained for Different Values of κ_e, the Kappa Index of the Lorentzian VDF of Coronal Electrons, for an Exobase Located at $r_0 = 2.5$ R$_s$ and an Exobase Temperature of $T_0 = 10^6$ K

κ_e	r_m, R$_s$	V_0, V	V_m, V	u, km s^{-1}
1000	6.690	685.7	338.1	182
5.0	4.465	947.8	723.1	277
3.0	3.677	1566.2	1411.5	439
2.5	3.476	2240.0	2110.7	565
2.2	3.370	3245.6	3133.4	713

Table 2. Values of r_m, the Radial Distance of the Maximum Total Potential Energy of the Protons, V_0, the Exobase Electric Potential, V_m, the Electric Potential at $r = r_m$ and u, the Solar Wind Bulk Speed at 1 AU Obtained for Different Values of the Exobase Level r_0 for a Kappa Index of the Electron VDF Given by $\kappa_e = 2.5$ and an Exobase Temperature of $T_0 = 10^6$ K

r_0, R$_s$	r_m, R$_s$	V_0, V	V_m, V	u, km s^{-1}
2.5	3.476	2240.0	2110.7	565
2.0	2.797	2771.9	2608.5	624
1.5	2.089	3725.1	3506.7	718
1.1	1.510	5221.4	4926.5	848

Table 3. Values of r_m, the Radial Distance of the Maximum Total Potential Energy of the Protons, V_0, the Exobase Electric Potential, V_m, the Electric Potential at $r = r_m$ and u, the Solar Wind Bulk Speed at 1 UA Obtained for Different Values of the Exobase Temperature T_0 for a Kappa Index of the Electron VDF Given by $\kappa_e = 2.5$ and an Exobase Level of $r_0 = 2.0$ R$_s$

T_0, K	r_m, R$_s$	V_0, V	V_m, V	u, km s^{-1}
1.0×10^6	2.797	2771.9	2608.5	624
1.3×10^6	2.775	2809.4	2648.3	635
1.5×10^6	2.750	2860.2	2701.0	646
2.0×10^6	2.667	3037.4	2884.4	680

account. This model is based on Lorentzian (Kappa) VDFs for the electrons and Maxwellian VDFs for the protons.

[29] The distribution of the interplanetary magnetic field is assumed to be radial for simplicity and because a spiral structure does not change significantly the density and bulk speed profiles [*Pierrard et al.*, 2001]. However, the use of a flux tube geometry similar to the one described in *Munro and Jackson* [1977] and very often used in MHD models has not yet been introduced in our kinetic models.

[30] When the exobase level r_0 is lower than r_m, the radial distance of the maximum of the proton potential energy, the protons are in an attractive potential at low altitude ($r < r_m$) where they are decelerated by the dominant gravitational field. Only the protons with high enough energy are able to overcome the total potential barrier and will be accelerated to supersonic velocities in the region $r > r_m$. We have shown that the lower the altitude of this exobase the larger the gravitational potential barrier limiting the escape flux of protons. Therefore the electric potential difference V_0 that keeps the escape fluxes of protons and electrons equal to each other is enhanced. Furthermore, the polarization electric field that maintains the electron and ion density scale heights equal and that ensures the plasma to be quasi-neutral, increases and strongly accelerates the solar wind to large bulk velocities at asymptotic distances.

[31] Our new exospheric model offers a simple physical explanation for the existence of high values of the bulk velocities observed in the fast solar wind which is known to originate from the coronal holes. Indeed, the density in the coronal holes is smaller so that the exobase is low. Also, the suprathermal electrons are overpopulated in the tails of the VDF, as it is indeed observed in the high speed solar wind. We have shown that an adequate combination of these two parameters in our model leads to bulk velocities ∼700–800 km/s, i.e., corresponding to the large values often observed in the high-speed solar wind. These results are obtained without taking unrealistic values for r_0, T_0 or κ_e. In particular, it does not require a large temperature at the exobase as in earlier hydrodynamics and exospheric solar wind models since the asymptotic value of the solar wind is not extremely sensitive to the value of T_0.

[32] For simplicity, we have assumed a single exobase for electrons and protons, which is only an approximation if the temperatures of electrons and protons are assumed identical. Indeed, with equal temperatures, the Coulomb mean free path of the electrons is smaller than that of the protons since they are related by

$$\lambda_e = 0.416\left(\frac{T_e}{T_p}\right)^2 \lambda_p. \tag{7}$$

Therefore in order to have the same exobase level for the electrons and the protons, the electron temperature should be 1.55 times larger than the temperature of the protons. This would increase the bulk velocity at large radial distance to higher values. However, recent SOHO measurements indicate that in the corona, the protons temperature is larger than the electrons temperature [e.g. *Esser et al.*, 1999]. Therefore more protons have enough kinetic energy to overcome the gravitational potential well and the polarization electric-field, ensuring the quasi-neutrality of the plasma is reduced. Consequently, the solar wind bulk speed is reduced by ∼20–40 km s^{-1} depending on the conditions chosen at the exobase. The case of multiple exobases for the different species is a rather complicated mathematical problem and has been solved by *Brandt and Cassinelli* [1966] only for the simplest case of a Pannekoek-Rosseland polarization electric field. Finally, note that if we assume $T_{p\|} > T_{p\perp}$ at the exobase, the bulk velocity would also increase to higher values.

[33] The main goal of this paper was to show that in the framework of this extended exospheric model of the solar wind, collisionless kinetic theory is able to reproduce the large bulk velocities observed in the fast solar wind, without ad hoc assumptions of hydrodynamical/fluid models about the rate of additional coronal heating and momentum transfer by wave-particle interactions.

Appendix A: Formulae for Protons Below r_m

[34] Since the gravitational and the electric forces balance each other at the radial distance r_m, we have to modify several parameters in the model of LS71:

$$V_\infty^2(r) = \psi_m - \psi(r)$$

$$X^2(r) = \psi_m - \psi(r) - \frac{\mu - 1}{\mu - \eta}(\psi_m - \psi_0),$$

where $\eta = B(r)/B(r_0)$ and $\mu = B(r)/B(r_m)$; ψ_m and ψ_0 are the dimensionless total potential of the protons r_m and r_0, respectively. With these definitions, $V_\infty^2(r)$ represents the minimum dimensionless energy that a proton at the altitude r should have in order to escape from the gravitational potential well. $X^2(r)$ is a dimensionless variable equal to 0 at r_0 and at r_m.

A1. Ballistic Protons

$$\begin{aligned} n^b(r) = n_0 \exp(-q) \Bigg\{ & 1 - \operatorname{erfc}(V_\infty) - A\left[1 - \operatorname{erfc}\left(\frac{X}{\sqrt{1-\eta}}\right)\right] \\ & - \frac{2}{\sqrt{\pi}} B\left[\exp\left(\frac{V_\infty^2}{\mu - 1}\right)\mathcal{D}\left(\frac{V_\infty}{\sqrt{\mu - 1}}\right) \right. \\ & \left. - \exp\left(\frac{X^2}{\mu - 1}\right)\mathcal{D}\left(\frac{X}{\sqrt{\mu - 1}}\right)\right]\Bigg\} \end{aligned} \tag{A1}$$

$$F^b(r) = 0 \tag{A2}$$

$$\begin{aligned} P_\|^b(r) = {} & n^b(r)kT_0 + n_0 kT_0 \exp(-q) \\ & \cdot\Bigg\{\eta A\left[1 - \operatorname{erfc}\left(\frac{X}{\sqrt{1-\eta}}\right) - \frac{2}{\sqrt{\pi}}\frac{X}{\sqrt{1-\eta}}\exp\left(\frac{-X^2}{1-\eta}\right)\right] \\ & + \mu B \frac{2}{\sqrt{\pi}}\left[\exp\left(\frac{V_\infty^2}{\mu-1}\right)\left(\mathcal{D}\left(\frac{V_\infty}{\sqrt{\mu-1}}\right) + \frac{V_\infty}{\sqrt{\mu-1}}\right) \right. \\ & \left. - \exp\left(\frac{X^2}{\mu-1}\right)\left(\mathcal{D}\left(\frac{X}{\sqrt{\mu-1}}\right) + \frac{X}{\sqrt{\mu-1}}\right)\right]\Bigg\} \end{aligned} \tag{A3}$$

$$P^b_\perp(r) = P^b_\parallel(r) - n_0 kT_0 \exp(-q)\left\{\frac{\eta q}{1-\eta} A\left[1 - \operatorname{erfc}\left(\frac{X}{\sqrt{1-\eta}}\right)\right]\right.$$
$$+ \frac{2}{\sqrt{\pi}}\frac{\mu V_\infty^2}{\mu - 1} B\left[\exp\left(\frac{V_\infty^2}{\mu-1}\right)\mathcal{D}\left(\frac{V_\infty}{\sqrt{\mu-1}}\right)\right.$$
$$\left.\left. - \exp\left(\frac{X^2}{\sqrt{\mu-1}}\right)\mathcal{D}\left(\frac{X}{\sqrt{\mu-1}}\right)\right]\right\} \quad (A4)$$

$$\epsilon^b(r) = 0. \quad (A5)$$

A2. Escaping Protons

$$n^e(r) = \frac{n_0}{2}\exp(-q)\left\{\operatorname{erfc}(V_\infty) - A\operatorname{erfc}\left(\frac{X}{\sqrt{1-\eta}}\right)\right.$$
$$\left. + \frac{2}{\sqrt{\pi}} B\left[\exp\left(\frac{V_\infty^2}{\mu-1}\right)\mathcal{D}\left(\frac{V_\infty}{\sqrt{\mu-1}}\right) - \exp\left(\frac{X^2}{\mu-1}\right)\mathcal{D}\left(\frac{X}{\sqrt{\mu-1}}\right)\right]\right\} \quad (A6)$$

$$F^e(r) = \frac{n_0}{4}\sqrt{\frac{8kT_0}{m\pi}}\left[\mu\exp(-q_m) + (\eta - \mu)\exp\left(\frac{-q_m}{1-\eta_m}\right)\right] \quad (A7)$$

$$P^e_\parallel(r) = \frac{1}{2} n^e(r) kT_0 + \frac{1}{2} n_0 kT_0 \exp(-q)$$
$$\cdot\left\{\eta A\left(\operatorname{erfc}\left(\frac{X}{\sqrt{1-\eta}}\right) + \frac{1}{\sqrt{\pi}}\frac{X}{\sqrt{1-\eta}}\exp\left(\frac{-X^2}{1-\eta}\right)\right)\right.$$
$$- \frac{\mu B}{\sqrt{\pi}}\left(\exp\left(\frac{X^2}{\mu-1}\right)\left[\mathcal{D}\left(\frac{X}{\sqrt{\mu-1}}\right) - \frac{X}{\sqrt{\mu-1}}\right]\right.$$
$$\left.\left. - \exp\left(\frac{-V_\infty^2}{\mu-1}\right)\left[\mathcal{D}\left(\frac{V_\infty}{\sqrt{\mu-1}}\right) - \frac{V_\infty}{\sqrt{\mu-1}}\right]\right)\right\} \quad (A8)$$

$$P^e_\perp(r) = P^e_\parallel(r) + \frac{1}{2} n_0 kT_0 \exp(-q)\left\{\frac{\eta q}{1-\eta} A\operatorname{erfc}\left(\frac{X}{\sqrt{1-\eta}}\right)\right.$$
$$- \frac{2}{\sqrt{\pi}}\frac{\mu V_\infty^2}{\mu-1} B\left[\exp\left(\frac{V_\infty^2}{\mu-1}\right)\mathcal{D}\left(\frac{V_\infty}{\sqrt{\mu-1}}\right)\right.$$
$$\left.\left. - \exp\left(\frac{X^2}{\mu-1}\right)\mathcal{D}\left(\frac{X}{\sqrt{\mu-1}}\right)\right]\right\} \quad (A9)$$

$$\epsilon^e(r) = \frac{n_0}{4}\sqrt{\frac{8kT_0}{\pi m}} kT_0 \exp(-q_m)\left\{\mu(2 + q_m - q)\right.$$
$$\left. - \exp\left(\frac{-\eta_m q_m}{1-\eta_m}\right)[(2-q)(\mu-\eta) + \mu q_m.]\right\} \quad (A10)$$

A3. Trapped Protons

$$n^t(r) = n_0\exp(-q)\left\{A\left(1 - \operatorname{erfc}\left(\frac{X}{\sqrt{1-\eta}}\right)\right)\right.$$
$$\left. - \frac{2}{\sqrt{\pi}} B\exp\left(\frac{X^2}{\mu-1}\right)\mathcal{D}\left(\frac{X}{\sqrt{\mu-1}}\right)\right\} \quad (A11)$$

$$F^t(r) = 0 \quad (A12)$$

$$P^t_\parallel(r) = n^t(r) kT_0 - n_0 kT_0 \exp(-q)$$
$$\cdot\left\{\eta A\left[1 - \operatorname{erfc}\left(\frac{X}{\sqrt{1-\eta}}\right) - \frac{2}{\sqrt{\pi}}\frac{X}{\sqrt{1-\eta}}\exp\left(\frac{-X^2}{1-\eta}\right)\right]\right.$$
$$\left. - \frac{2}{\sqrt{\pi}}\mu B\exp\left(\frac{X^2}{\mu-1}\right)\left[\mathcal{D}\left(\frac{X}{\sqrt{\mu-1}}\right) - \frac{X}{\sqrt{\mu-1}}\right]\right\} \quad (A13)$$

$$P^t_\perp(r) = P^t_\parallel(r) + n_0 kT_0 \exp(-q)\left\{\frac{\eta q}{1-\eta} A\left[1 - \operatorname{erfc}\left(\frac{X}{\sqrt{1-\eta}}\right)\right]\right.$$
$$\left. - \frac{2}{\sqrt{\pi}}\frac{\mu V_\infty^2}{\mu-1} B\exp\left(\frac{X^2}{\mu-1}\right)\mathcal{D}\left(\frac{X}{\sqrt{\mu-1}}\right)\right\} \quad (A14)$$

$$\epsilon^t(r) = 0. \quad (A15)$$

[35] The definition of the complementary error function and Dawson's integral are

$$\operatorname{erfc}(x) = \frac{2}{\sqrt{\pi}}\int_x^\infty \exp(-t^2)dt$$

$$\mathcal{D}(x) = \exp(-x^2)\int_0^x \exp(t^2)dt$$

[36] These functions are related to the $K_m(x)$ and $W_m(x)$ functions introduced in *LS71* by the following relations:

$$K_m(x) = \frac{1}{2}(m-1)K_{m-2}(x) - \frac{x^{m-1}}{\sqrt{\pi}}\exp(-x^2)$$
$$K_0(x) = 1 - \operatorname{erfc}(x)$$
$$K_1(x) = \frac{1}{\sqrt{\pi}}\left[1 - \exp(-x^2)\right]$$

$$W_m(x) = \frac{x^{m-1}}{\sqrt{\pi}}\exp(x^2) - \frac{1}{2}(m-1)W_{m-2}(x)$$
$$W_0(x) = \frac{2}{\sqrt{\pi}}\exp(x^2)\mathcal{D}(x)$$
$$W_1(x) = \frac{1}{\sqrt{\pi}}\left[\exp(x^2) - 1.\right]$$

[37] Moreover, for convenience, the following dimensionless variables have also been introduced:

$$q = \psi - \psi_0 \qquad q_m = \psi_m - \psi_0$$
$$A = \sqrt{1-\eta}\exp\left(-\frac{\eta q}{1-\eta}\right) \qquad B = \sqrt{1-\mu}\exp\left(-\frac{\mu V_\infty^2}{\mu-1}\right).$$

Appendix B: Formulae for Protons Beyond r_m

[38] To calculate the moments of the escaping particles above r_m, we integrate the VDF of the protons over a domain of velocity space defined by

$$\left[\sqrt{v_m^2 - v_\psi^2}, \infty\right] \qquad [0, \theta_M],$$

from which we remove the new empty domain defined by

$$[v_b, \infty] \qquad [\theta_m, \theta_M].$$

[39] These limits of the velocity space are defined in polar coordinates. v_b corresponds to the intersection of hyperbolae θ_M and θ_m illustrated in Figure 2.

[40] The following definitions have been used:

$$\sin^2\theta_M = \mu\left(1 - \frac{\psi_m - \psi}{V^2}\right)$$

$$\sin^2\theta_m = \eta\left(1 + \frac{\psi - \psi_0}{V^2}\right)$$

$$V^2 = \frac{mv^2}{2kT} \qquad V_\psi^2 = \psi$$

$$V_m^2 = \psi_m \quad V_b^2 = \frac{q_m}{1-\eta_m} - q$$

$$\eta_m = B(r_m)/B(r_0).$$

[41] Unlike in the article of *Lemaire* [1976], the mathematical expressions for the moments of the protons VDF are formulated in terms of the complementary error function and Dawson's integral. It has been checked that these expressions are consistent with formulae (18), (30) and (31) of *Lemaire* [1976] and with the general formulae (7)–(9) of *Khazanov et al.* [1998].

$$n(r) = \frac{1}{2}n_0\exp(-q)\Big\{\mathrm{erfc}\left(V'_M\right) - A\,\mathrm{erfc}\,(Y_M) - B'\left(\mathrm{erfc}\left(X'_M\right) - \mathrm{erfc}\left(X_M\right)\right)\Big\} \tag{B1}$$

$$F(r) = \frac{n_0}{4}\sqrt{\frac{8kT_0}{m\pi}}\left[\mu\exp(-q_m) + (\eta-\mu)\exp\left(\frac{-q_m}{1-\eta_m}\right)\right] \tag{B2}$$

$$\begin{aligned}P_\parallel(r) = {} & n(r)kT_0 + \frac{1}{2}n_0kT_0\exp(-q)\\ & \cdot\Bigg\{\eta A\left[\mathrm{erfc}(Y_M) + \frac{2}{\sqrt{\pi}}Y_M\exp\left(-Y_M^2\right)\right]\\ & -\mu B'\left[\left(\mathrm{erfc}(X_M) + \frac{2}{\sqrt{\pi}}X_M\exp\left(-X_M^2\right)\right)\right.\\ & \left.-\left(\mathrm{erfc}\left(X'_M\right) + \frac{2}{\sqrt{\pi}}X'_M\exp\left(-X'^2_M\right)\right)\right]\Bigg\}\end{aligned} \tag{B3}$$

$$\begin{aligned}P_\perp(r) = {} & P_\parallel - n_0kT_0\exp(-q)\\ & \cdot\left\{\frac{\eta q}{1-\eta}A\,\mathrm{erfc}(Y_M) - \frac{\mu V'^2_M}{1-\mu}.B'\left[\mathrm{erfc}\left(X'_M\right) - \mathrm{erfc}(X_M)\right]\right\}\end{aligned} \tag{B4}$$

$$\begin{aligned}\epsilon(r) = {} & \frac{n_0}{4}kT_0\left(\frac{8kT_0}{m\pi}\right)^{1/2}\exp(-q_m)\Big\{\mu(2+q_m-q).\\ & -\exp\left(\frac{-\eta_m q_m}{1-\eta_m}\right)[(2-q)(\mu-\eta) + \mu q_m],\Big\}\end{aligned} \tag{B5}$$

where the following variables are defined according to *Lemaire*'s [1976] work by

$$V'^2_M = q_m - q \tag{B6}$$

$$Y_M^2 = \frac{q_m}{1-\eta_m} - \frac{q}{1-\eta} \tag{B7}$$

$$X_M^2 = \frac{q_m - q}{1-\mu} + \frac{\eta_m q_m}{1-\eta_m} \tag{B8}$$

$$X'^2_M = \frac{q_m - q}{1-\mu}. \tag{B9}$$

[42] These variables are related to those defined above for the case $r < r_m$ by

$$\begin{aligned}V'_M &= V_\infty\\ Y_M^2 &= \frac{X^2}{1-\eta}\\ X_M^2 &= \frac{X^2}{1-\mu}\\ X'^2_M &= \frac{V_\infty^2}{1-\mu}.\end{aligned}$$

[43] Note that we have introduced in equations (B1)–(B5) the parameter $B' = \sqrt{1-\mu}\,\exp\left(\frac{-\mu(q-q_m)}{1-\mu}\right)$ instead of the parameter B, defined for the case $r < r_m$, since at altitudes above r_m, the variable μ becomes larger than 1.

[44] When $r = r_m$, it can be verified that $\eta = \eta_m$, $\mu = 1$, $q = q_m$, $n^b = n^t = 0$, and the mathematical expression for the number density of the escaping particles, given by formulae (A6) and (B1), are continuous at r_m. The other moments and their first derivatives are also continuous at $r = r_m$.

[45] Note that all these expressions have been normalized so that n_0 corresponds to the actual density at the exobase.

[46] **Acknowledgments.** H. Lamy and V. Pierrard thank the Belgian FNRS and the SSTC (Service des Affaires Scientifiques, Techniques et Culturelles) for their support. The authors also would like to thank K. Jockers for important and useful discussions about this work.

[47] Shadia Rifai Habbal thanks Hans J. Fahr and S. Peter Gary for their assistance in evaluating this paper.

References

Brandt, J. C., and J. P. Cassinelli, Interplanetary gas, 11, An exospheric model of the solar wind, *Icarus*, *5*, 47, 1996.

David, C., A. H. Gabriel, F. Bely-Dubau, A. Fludra, P. Lemaire, and K. Wilhelm, Measurement of the electron temperature gradient in a solar coronal hole, *Astron. Astrophys.*, *336*, L90, 1998.

Esser, R., L. Fineshi, D. Dobrzycka, S. R. Habbal, R. J. Edgar, J. C. Raymond, and J. L. Kohl, *Appl. J.*, *510*, L63, 1999.

Fahr, J. H., and B. Shizgal, Modern exospheric theories and their observational relevance, *Rev. Geophys.*, *21*, 75, 1983.

Jockers, K., Solar wind models based on exospheric theory, *Astron. Astrophys.*, *6*, 219, 1970.

Khazanov, G. V., M. W. Liemohn, E. N. Krivorutsky, and T. E. Moore, Generalized kinetic description of a plasma in an arbitrary field-aligned potential energy structure, *J. Geophys. Res.*, *103*, 6871, 1998.

Lemaire, J., Rotating ion exospheres, *Planet. Space Sci.*, *24*, 975, 1976.

Lemaire, J., and V. Pierrard, Kinetic models of solar and polar winds, *Astrophys. Space Sci.*, *277*, 169, 2001.

Lemaire, J., and M. Scherer, Kinetic models of the solar wind, *J. Geophys. Res.*, *76*, 31, 1971a.

Lemaire, J., and M. Scherer, Simple model for an ion-exosphere in an open magnetic field, *Phys. Fluids*, *14*, 1683, 1971b.

Lemaire, J., and M. Scherer, Kinetic models of the solar and polar winds, *Rev. Geophys.*, *11*, 427, 1973.

Liehmon, M. W., and G. V. Khazanov, Collisionless plasma modeling in an arbitrary potential energy distribution, *Phys. Plasmas*, *5*, 580, 1998.

Maksimovic, M., V. Pierrard, and P. Riley, Ulysses electron distributions fitted with Kappa functions, *Geophys. Res. Let.*, *24*, 1151, 1997a.

Maksimovic, M., V. Pierrard, and J. Lemaire, A kinetic model of the solar wind with Kappa distributions in the corona, *Astron. Astrophys.*, *324*, 725, 1997b.

Maksimovic, M., V. Pierrard, and J. Lemaire, On the exospheric approach for the solar wind acceleration, *Astrophys. Space Sci.*, *277*, 181, 2001.

Munro, R. H., and B. V. Jackson, Physical properties of a polar coronal hole from 2 to 5 Rs, *Appl. J.*, *213*, 874, 1977.

Pierrard, V., and J. Lemaire, Lorentzian ion exosphere model, *J. Geophys. Res.*, *101*, 7923, 1996.

Pierrard, V., M. Maksimovic, and J. Lemaire, Electron velocity distribution function from the solar wind to the corona, *J. Geophys. Res.*, *104*, 17,021, 1999.

Pierrard, V., K. Issautier, N. Meyer-Vernet, and J. Lemaire, Collisionless model of the solar wind in a spiral magnetic field, *Geophys. Res. Lett.*, *28*, 223, 2001.

Scherer, M., On the numerical evaluation of the complementary error function and Dawson's integral, *Aeronom. Acta*, *6*, 1, 1972.

Spitzer, L., Jr., *Physics of Fully Ionized Gases*, Wiley-Interscience, New York, 1962.

Whitbroe, G. L., The temperature structure, mass, and energy flow in the corona and inner solar wind, *Appl. J.*, *325*, 442, 1988.

H. Lamy, V. Pierrard, and J. F. Lemaire, Institut d'Aéronomie Spatiale de Belgique, 3 Avenue Circulaire, B-1180 Brussels, Belgium. (herve.lamy@oma.be; viviane.pierrard@oma.be; joseph.lemaire@oma.be)

M. Maksimovic, LESIA, Observatoire de Paris, 92195 Meudon Principal Cedex, France. (milan.maksimovic@obspm.fr)